Jurnal Tribologi 49 (2026) 95-115

MYTRIBOS Malaysian Tribology Society

Jurnal Tribologi

Website : jurnaltribologi.mytribos.org e-issn: 2289-7232

Steady-state performance analysis of macro-grooved hydrodynamic journal-bearing

Arun Bangotra *, Sanjay Sharma

School of Mechanical Engineering, Shri Mata Vaishno Devi University, Katra, 182320 Jammu and Kashmir, INDIA.
*Corresponding author: arunbangotra@gmail.com

KEYWORDS

Textures
Reynolds's equation
Finite element method
Journal bearing
Load-carrying capacity
Friction coefficient

ABSTRACT

This study investigates the static performance characteristics of the journal bearing with rectangular macro-groove textures. The static characteristics like load carrying capacity (LCC) and friction coefficient (FC) are determined using the finite element method by solving the governing Reynolds's equation of lubricant flow. The effect of rectangular macro-groove textures provided in specific regions of the journal bearing – the full, the first half, the second half, and the increasing pressure region – along with variations in groove depth and area density, is investigated at different eccentricity ratios. From the simulated results, the static characteristics of the journal bearing are enhanced as the eccentricity ratio increases from lower to higher values. At the lower eccentricity ratio of 0.2, the maximum enhancement of LCC is 95.75%, and a 48.67% reduction in FC is found with four rectangular macro-groove textures with an area density of 58.50% and a non-dimensional groove depth of 0.9 placed in the pressure-increasing region. However, at a higher eccentricity ratio of 0.8, the promotion of macro-groove textures, the maximum performance was found at the optimum geometry of one groove in the pressure-increasing region, at a depth of 0.3, as LCC enhances by 1.72% and FC reduces by 1.46%.

Received 4 February 2025; received in revised form 31 July 2025; accepted 14 August 2025.
To cite this article: Bangotra and Sharma (2026). Steady-state performance analysis of macro-grooved hydrodynamic journal-bearing. Jurnal Tribologi 49, pp.95-115.

1.0 INTRODUCTION

In mostly fast-speed rotational machinery like turbines, pumps, motors and other rotating machines, journal bearings are widely employed to support radial loads for a wide range of operating conditions. Modifications to the surface topology of the bearing profile, such as surface waviness, micro and macro-texturing, grooves etc. as observed by different researchers have an impact on the bearing's efficient operation. Several modern manufacturing techniques, like casting, etching, laser surface texturing/grooving etc. available now a days have made it possible to produce machine parts more accurately. Today, surface texturing or grooving is crucial for safe and effective bearing operations. Moreover, to enhance the bearing performance, a designer must choose the appropriate micro/macro-texture distribution and its shape. The textured region acts as lubricant reservoir and enhances the nominal lubricant film thickness and minimizes the friction between two lubricating surfaces as textured or grooved area provides an enhanced clearance between journal and bearing surface thereby improving the performance of bearing.

As a result, many studies in past few years have explored the effects of various geometrical parameters such as shapes of textures/grooves, size and area density. Qiu et al., 2013 investigated the effects of commonly used dimple forms on gas-lubricated slider bearings and discovered that the maximum performance is achieved by an ellipsoidal dimple. Some authors, (Wang and He, 2019) reported that the herringbone grooves affected the performance of journal bearing and the groove's tip produces the most pressure and can lower the outlet's average axial velocity. According to Uddin and Liu, 2016, a star-like texture lowers the friction coefficient more than a triangle, circle, ellipse, or chevron shaped textures on the bearing surface. Kango et al., 2014 determined that micro-grooving reduces the average temperature and enhances the friction coefficient when compared to spherical texture. Arif et al., 2022 discovered that a well-chosen lubricant rheology, slip boundary condition, and micro-texture all work together to improve the hydrodynamic lubrication film stability in journal bearings. To increase the load capacity and reduce friction, authors (Zhang et al., 2021) employed a multi objective optimization method using a non-dominated sorting genetic algorithm (NSGA) to adjust the texture characteristics of the micro-grooved journal bearing. According to Ashihara and Hashimoto, 2010, the performance of micro-grooved bearing under mixed lubrication circumstances is influenced by the depth of the microgroove. Adatepe et al., 2013 explored the effect of micro-grooved and for superior tribological performance; they identified the circular grooved journal bearing's ideal design characteristics. Yu et al., 2016 claimed that the characteristics of flexible bearing with texturing depend upon the number of textures, its depth and location.

Further many researchers have explored the effects of partial texturing on the bearing regions. According to Fu et al., 2012, a partial texturing slider with orientation grooves parabolic with infinite width, the lubricant pressure depends upon the orientation angle of groove, density area and depth. Shinde et al., 2017 determined the optimal configuration for journal bearings with partial micro-grooves. Tala-Ighil et al., 2011 investigated the operation of textured journal bearings with spherical and cylindrical distributions. They determined that entire texture regions had a negative impact on journal bearing performance while partial texture regions had a positive effect. Authors (Sharma et al., 2019; Sharma et al., 2021) used the finite element analysis to investigate the effect of triangular and v-shaped textures on the hydrodynamic journal bearing and reported that load carrying-capacity enhances and friction coefficient reduces with an increase in the textured depth when it is located in an area of increasing pressure. Jamwal et al., 2020 studied the dynamic characteristics of chevron textures with different depths and observed that these factors influence the performance of the bearing. Khatri and Sharma, 2016 reported

that the fully spherical textured hybrid bearing has lower frictional torque in comparison to partial textured. Rao et al., 2013 examined the impact of partial texturing and a trapezoidal depression on load carrying-capacity of bearing. According to Gui and Meng, 2019, the static characteristics of a bearing are enhanced when its dimples are located in its pressure-rising part and the load capacity is increased together with the friction force by the spikes at the pressure-falling zone. Singh and Awasthi, 2022 reported increased performance metrics of the cylindrical, spherical, triangle, and kite-textured bearings when the texture distribution occurs in the bearing's pressure-rising zone.

Chen et al., 2020 determined the best geometrical parameters for the partially textured bearings with circular grooves to maximize their load-carrying capacity. Feng et al., 2021 analyzed the water-lubricated grooved journal bearing and discovered that the groove texture parameters have an impact on the load capacity and significantly raise the load capacity at high rotational speed and less eccentricity ratio. By using numerical investigation, Sharma and Tomar, 2021 showed that the bearing system's stability and minimal fluid layer thickness are increased due to micro-grooves and magneto rheological fluid.

Pattnayak et al., 2022 reported significant static and dynamic performance improvements due to the presence of bionic textures fused micro-pocketed bores in comparison to conventional bores. Rahmani et al., 2018 explore the reduction of coefficient of friction in a powder-lubricated journal bearing employing different pocket shapes (elliptical, parabolic, rectangular, and trapezoidal) placed on bore surface. They found that the journal bearing having rectangular pocket yields least coefficient of friction among all the cases. Kumar and Sharma, 2019 looked into the performance of hybrid thrust bearings with micro-grooves of trapezoidal, triangular, circular, and rectangular geometries. They discovered that rectangular grooves offer the highest load carrying capacity at the optimum value for groove width and depth. Li et al., 2021 investigated the impact of various bottom profiles of square textured bearings and reported that flat bottom yield maximum static performance of journal bearing.

Sharma and Kushare, 2017 studied the impact of the orientation pattern of a two-lobe hybrid bearing and found that a proper surface pattern improves the stability of the bearing. Further, studies by (Sahu and Sharma, 2018; Bangotra and Sharma, 2022; Bangotra and Sharma, 2023; Sharma et al., 2012; Manser et al., 2019) revealed various other 3-dimensional irregularities, including the non-circularity of bearing, surface waviness, texturing with misalignment and the journal shapes influence the static characteristics of bearing.

After a through literature review, it has been observed that while micro-texturing of bearing surfaces has been extensively studied in the past two decades, there exists a noticeable research gap regarding the use of macro-groove surface textures, particularly those with rectangular geometries, in journal bearings. Previous studies have largely limited their investigations to grooves placed in the pressure-increasing (converging) zone only. However, other groove placements - such as full, first-half, and second-half regions and their implications on bearing performance have not been systematically explored. Furthermore, there is limited literature analyzing the influence of key groove design parameters (number, depth, and area density) across a wide range of eccentricity ratios (0.2 to 0.8), especially for macro-textured surfaces. The present work aims to fill this research gap by investigating the impact of rectangular macro-groove textures on different bearing regions and identifying optimum texture configurations for enhanced static performance characteristics (load carrying capacity, friction coefficient, etc.). This study contributes to the field by offering new insights into how macro-texture placement and

geometry influence the lubrication characteristics of hydrodynamic journal bearings- which can assist designers in achieving improved bearing performance under varied operating conditions.

2.0 MATHEMATICAL MODELLING

Figure 1(a) and (b) show the cross-sectional view and geometrical parameters of rectangular macro-grooved hydrodynamic journal bearing (MGHJB) model considered in the present study. In this analysis, boundary conditions are implemented at the supply hole to account for the inlet oil. The oil hole is represented as area with predetermined flow rate and oil is assumed to be provided at a steady pressure. Our study focuses on a particular application where a single supply hole lubrication system is ideally suited for the working circumstances, which include moderate loads and speeds to ensure the ideal possible oil distribution and efficient lubrication as reported by (Sharma and Kushare, 2017).

For a journal bearing system working at steady state regime, the non-dimensional form of the Reynolds equation to determine the pressure distribution of thin viscous fluid layers, assuming that the flow is incompressible and laminar, fluid is Newtonian and iso-viscous given by (Tala-Ighil et al., 2011; Sharma et al., 2019) as under:-

$$\frac{\partial}{\partial\alpha}\left[\bar{h}^3\overline{F}_2\left(\frac{\partial\bar{p}_t}{\partial\alpha}\right)\right]+\frac{\partial}{\partial\beta}\left[\bar{h}^3\bar{F}_2\left(\frac{\partial\bar{p}_t}{\partial\beta}\right)\right]=\bar{\Omega}\left[\frac{\partial}{\partial\alpha}\left\{\left(1-\frac{\bar{F}_1}{\bar{F}_0}\right)\bar{h}\right\}\right]+\frac{\partial\bar{h}}{\partial\bar{t}} \quad (1)$$

where, $\bar{F}_0, \bar{F}_1$ and $\bar{F}_2$ are viscosity integrals are expressed as:-

$$\bar{F}_0=\int_0^1\frac{1}{\bar{\mu}}d\bar{z}, \bar{F}_1=\int_0^1\frac{\bar{z}}{\bar{\mu}}d\bar{z} \text{ and } \bar{F}_2=\int_0^1\frac{\bar{z}}{\bar{\mu}}\left(\bar{z}-\frac{\bar{F}_1}{\bar{F}_0}\right)d\bar{z} \quad (2)$$

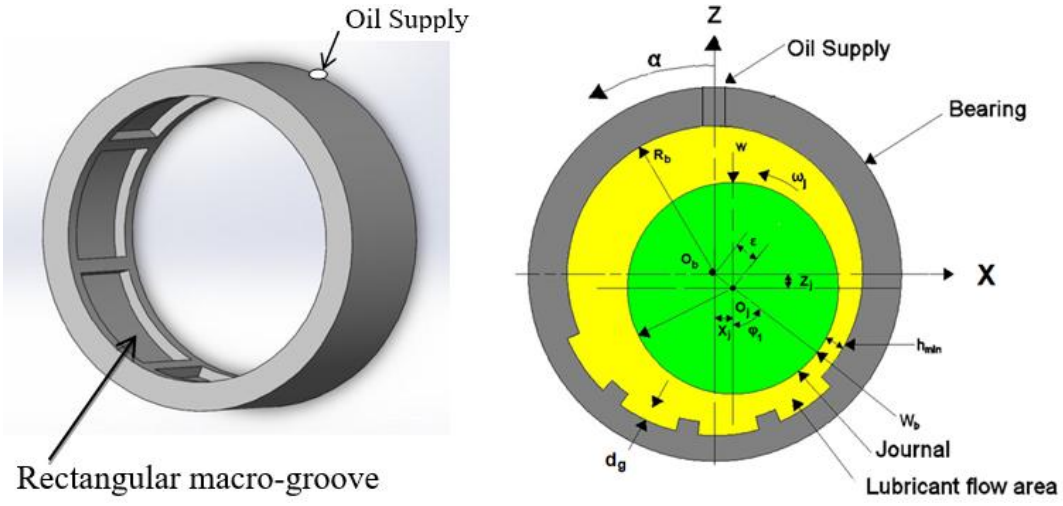

Figure 1: Sectional view (a) 3-Dimensional and (b) 2-Dimensional of macro-grooved hydrodynamic journal bearing (MGHJB) and co-ordinate system.

2.1 Nominal Lubricant Film Thickness

The journal bearing's lubricant film thickness in non-dimensional form used in Equation (1) to determine the lubricant pressure distribution in the clearance space as defined by (Sharma et al., 2019; Singh and Awasthi, 2022) as under:-

$$\bar{h} = (1 - \bar{X}_j \cos\alpha - \bar{Z}_j \sin\alpha) + \bar{h}_g \quad (3)$$

where, $\bar{h}$ is the non-dimensional fluid film thickness in plain circular smooth rigid bearing which is equal to $\bar{h} = h/c_r$; where 'h' is the fluid-film thickness in mm and $c_r$is radial clearance i.e R_b - R_j in mm. R_b and R_j are the radius of bearing and journal respectively. In the above equation, $\bar{X}_j$and$\bar{Z}_j$ defines the steady-state journal center co-ordinates, and $\bar{h}_g$ is the variation in film thickness due to presence of the macro-groove in the considered regions and is defined (Qiu et al., 2013; Manser et al., 2019) as under:-

For non-groove region;

$$\bar{h}_g = 0 \text{if}(x_0, y_0) \notin \psi; \quad (4)$$

For rectangular macro-groove region;

$$\bar{h}_g = \bar{d}_g \text{ if}(x_0, y_0) \in \psi; \quad (5)$$

where;

$\psi = \begin{Bmatrix} x_0 \geq \alpha_b and x_0 \leq \alpha_e \\ y_0 \geq \beta_b and y_0 \leq \beta_e \end{Bmatrix}$
$\bar{d}_g =$ Non-dimensional depth of groove
$\alpha_u =$ Unit cell angle of macro-groove $= 90^0$(Four rectangular macro-groove)
$\alpha_b =$ Starting angle of macro-groove $= 0.125\alpha_u$
$\alpha_e =$ Ending angle of macro-groove $= 0.875\alpha_u$
$\beta_b, \beta_b =$ Macro $-$ groove dimension in axial direction $= \pm 0.75$
$\alpha = 0 - 360^0$; for full region
$\alpha = 0 - 180^0$; for 1st half region
$\alpha = 180^0 - 360^0$; for 2nd half region
$\alpha = 144^0 - 288^0$; for pressure enhancing region

where, x_0 and y_0 define the local coordinates of the groove. $\bar{d}_g$defines the non-dimensional depth of the macro-groove texture related to the radial bearing clearance i.e $\bar{d}_g = d_g/c_r$. The macro-groove regions on bearing surface as mentioned above as defined in the Equation (4) have been chosen from the pressure profile of the plain bearing and published literature (Gui and Meng, 2019; Sharma et al. 2021) to place the rectangular macro-groove as depicted in Figure 3(a)–(d). One groove length consists of 90^0, 45^0 and 36^0 in case of four rectangular macro-grooves placed in the full region, first or second half region and pressure enhancing region as displayed in Figure 3(a)–(d).

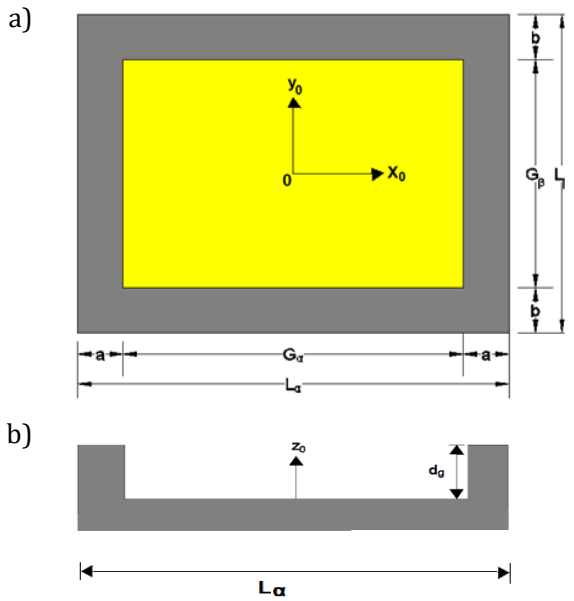

Figure 2: (a) Top View (b) Front view of rectangular macro-groove on bearing surface.

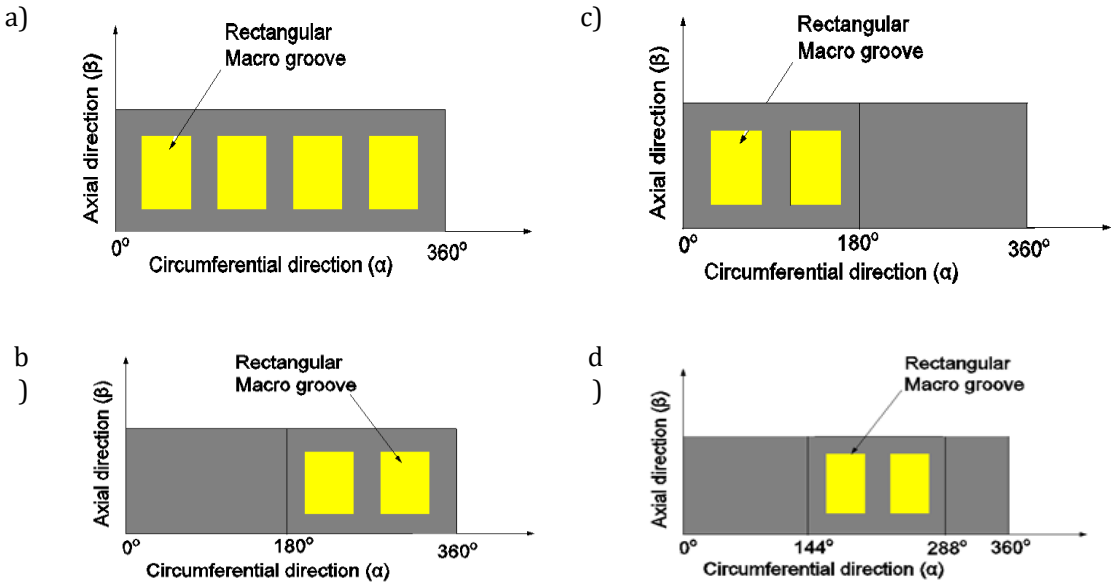

Figure 3: (a) Distribution of rectangular macro-grooves on (a) Bearing entire surface (0–3600); (b) Bearing first half (0-1800); (c) Bearing bottom half (180–3600); (d) Bearing pressure-increasing region (144-2880).

2.2 Finite Element Method

The non-dimensional Reynolds Equation (1) has been mathematically solved by using the finite element method. In order to discretize the lubricant flow domain, four nodded quadrilateral elements are used and the variation of film pressure along the two principal axis ζ and η is expressed as:-

$$\bar{p}_t = \sum_{j=1}^{n_e} N_j \bar{P}_j \; ; N_j = \frac{(1+\zeta_i\zeta)(1+\eta_i\eta)}{4} \tag{6}$$

where, N_j is the shape factor of elements and n_e are the total number of nodes in each element. After substitution of the pressure values in the Reynolds equation, this leads to generation of residue error (R^e). To minimize this residue over the whole flow domain, the weak formulation of Reynolds Equation (1) has been done by using the Galerkin's technique, described as:-

$$\begin{aligned} &\frac{\partial}{\partial\alpha}\left[\bar{h}^3\overline{F}_2\frac{\partial}{\partial\alpha}\left(\sum_{j=1}^{4}N_j\bar{P}_j\right)\right]+\frac{\partial}{\partial\beta}\left[\bar{h}^3\bar{F}_2\frac{\partial}{\partial\beta}\left(\sum_{j=1}^{4}N_j\bar{P}_j\right)\right] \\ &-\bar{\Omega}\left[\frac{\partial}{\partial\alpha}\left\{\left(1-\frac{\bar{F}_1}{\bar{F}_0}\right)\bar{h}\right\}\right]-\frac{\partial\bar{h}}{\partial\bar{t}}=R^e \end{aligned} \tag{6}$$

In Galerkin's approach, the shape function of pressure, which is the primary variable, has been used as the weight itself. The above equation after simplification can be written in an algebraic equation in the matrix form expressed by (Khatri and Sharma, 2016) as under:-

$$\sum_{e=1}^{n_e}[[\bar{F}_M]^e\{\bar{p}_V\}^e]=\sum_{e=1}^{n_e}\left[\{\bar{Q}_V\}^e+\bar{\Omega}\{\bar{R}_H\}^e+\dot{\bar{X}}_j\{\bar{R}_{Xj}\}^e+\dot{\bar{Z}}_j\{\bar{R}_{Zj}\}^e\right] \tag{7}$$

For the eth element, for the Newtonian lubricant, the matrix and column vectors are expressed as:-

$$\bar{F}^e{}_{Mij}=\int_{A^e}\int\left\{\frac{\bar{h}^3}{12\bar{\mu}}\left(\frac{\partial N_{Vi}}{\partial\alpha}\frac{\partial N_{Vj}}{\partial\alpha}+\frac{\partial N_{Vi}}{\partial\beta}\frac{\partial N_{Vj}}{\partial\beta}\right)\right\}d\alpha d\beta$$

$$\bar{Q}_{V_i}{}^e=\int_{\Gamma^e}\left\{\left(\frac{\bar{h}^3}{12\bar{\mu}}\frac{\partial\bar{p}_V}{\partial\alpha}-\frac{1}{2}\bar{\Omega}\bar{h}\right)n_1+\left(\frac{\bar{h}^3}{12\bar{\mu}}\frac{\partial\bar{p}_V}{\partial\beta}\right)n_2\right\}N_{Vi}d\bar{\Gamma}^e$$

$$\bar{R}^e{}_{Hi}=\int_{A^e}\int\frac{1}{2}\bar{h}\frac{\partial N_{Vi}}{\partial\alpha}d\alpha d\beta$$

$$\bar{R}^e{}_{Xji}=\int_{A^e}\int cos\,\alpha\,N_{Vi}\,d\alpha d\beta$$

$$\bar{R}^e{}_{Xzi}=\int_{A^e}\int sin\,\alpha\,N_{Vi}\,d\alpha d\beta$$

The directional cosines in each direction (α and β) are indicated by n_1 and n_2, while i, j =1, 2… n^e and, $\bar{\Omega}$ = Speedparameter,$\omega_j\mu_r{R_j}^2/{c_r}^2p_{st}$.

2.3 Boundary Conditions

To solve the Reynolds equation, the Reynolds boundary conditions of the variable $\bar{p}_t$ and its derivative are used in the domain of lubricant flow (Sharma et., 2021). Implementing the FEM with the JFO (Jakobsson-Floberg-Olsson) boundary condition in MATLAB presents certain challenges due to the complexity of the boundary condition and the limitations of available tools. Hence in our study Reynolds boundary condition are used as a practical starting point, given its broad application and ease of implementation in MATLAB. However, we recognize the potential advantages of using the JFO boundary condition for more accurate results, as it captures the detailed behaviour of the lubrication film more effectively. In light of this, we encourage future researchers to explore the integration of JFO boundary conditions into their FEM models, particularly in MATLAB, by either customizing their approach or leveraging any available advanced solvers or toolboxes.

In our present study, the following Reynold's boundary conditions due to its widespread use in similar analyses are taken (Sharma and Kushare, 2017; Singh and Awasthi, 2022):

- On the two ends of the bearings, i.e. at the leading edges, the value of the pressure is taken as atmospheric pressure.
- At all nodes on the bearing boundary's external edges, pressure is assumed to be zero.
$$\bar{p}_t = 0.0 \text{at} \beta = \pm 1.0$$
- The boundary condition considers the effect of cavitation by assuming the pressure gradient to be zero at the trailing edges of the positive region:
$$\bar{p}_t = \frac{\partial \bar{p}_t}{\partial \alpha} = 0.0$$

2.4 Steady-state Performance Characteristics

2.4.1 Load carrying capacity (LCC)

The lubricant-film reaction components given by (Khatri and Sharma, 2016) as under:-

$$\bar{W}_x = -\int_{-\lambda}^{\lambda}\int_{0}^{2\pi} \bar{p}_t \cos\alpha \, d\alpha d\beta$$
$$\bar{W}_z = -\int_{-\lambda}^{\lambda}\int_{0}^{2\pi} \bar{p}_t \sin\alpha \, d\alpha d\beta \quad (8)$$

The attitude angle and load carrying-capacity is determined as:-

$$\phi = tan^{-1}\left(\frac{\overline{W}_z}{\overline{W}_x}\right)$$
$$\bar{W}_b = \sqrt{(\bar{W}_x)^2 + (\bar{W}_z)^2} \quad (9)$$

2.4.2 Friction coefficient (FC)

The ratio of frictional force to load carrying-capacity (LCC) yields the friction coefficient (FC). The values are taken in non-dimensional form. The frictional force given by (Khatri and Sharma, 2016) is as under:-

$$\bar{F}_L = \sum_{e=1}^{n_e} \int_{A^e} \left(\Omega \frac{\bar{\tau}_c}{\bar{h}} + \frac{\bar{h}}{2} \frac{\partial \bar{p}}{\partial \alpha} \right) dA \tag{10}$$

where $\bar{\tau}_c$ is the Couette shearing stress = 1.0 for laminar flow. The non-dimensional value of friction coefficient (FC) of lubricant fluid film is calculated as under:-

$$\bar{f} = \frac{\bar{F}_L}{\bar{W}_b} \tag{11}$$

3.0 COMPUTATIONAL PROCEDURE

By using the overall solution procedure as shown in Fig. (4), the static characteristics of macro-groove journal bearing (MGJB) were computed. The various geometric and operational bearing input parameters are given in Table 2. Equation (1) is solved using the finite element analysis with the help of MATLAB program. To solve the system of equations in order to obtain the nodal pressure at every gauss point in the discretized fluid domain of lubricant, Gauss-Seidel methodology has been adopted. In the present finite element method (FEM)-based simulation of the hydrodynamic journal bearing, the convergence of the solution has been monitored at the nodal level. Specifically, convergence is achieved when the pressure values at the nodes exhibit negligible change between successive iterations, ensuring numerical stability and accuracy of the solution. This approach is standard in FEM analyses, as nodal values directly represent the primary variables (e.g., pressure) in the discretized domain.

The subsequent prerequisites are tested for every node after calculating vector values $\{\bar{P}_0\}$ and $\{\bar{Q}\}$ from Equation (7):-

- Nodes are in the cavitation zone, $\{\bar{Q}\}<0$;
- Nodes are in the lubricating flow zone, $\{\bar{P}_0\}> 0$.

Solutions will exist if these criteria are met; if not, nodes that don't fit the criteria will be moved to another place and the calculation process will keep going until a solution is found. In journal bearing analysis, either external load or eccentricity ratio (ε) are taken as the primary input. In the present study, the eccentricity ratio is taken as an input, and the corresponding load carrying capacity (LCC) is computed based on the pressure distribution developed in the lubricant film. This approach is chosen to systematically investigate how variations in macro-groove geometry and placement influence the bearing's performance at different eccentricity ratios — which represent various operational states of the bearing. Since eccentricity ratio (ε) is a normalized measure of the journal's position inside the bearing clearance, it provides a convenient and dimensionless way to control the operating condition during simulations. The LCC is then obtained as an output, representing the capacity of the bearing to support load for that specific eccentricity and groove configuration. For a specified, eccentricity ratio, ε and given bearing

parameters as mentioned in Table 3, the journal center coordinates are initially estimated for a tentative attitude angle. Using these coordinates, the film thickness and pressure distribution are computed. From the pressure field, the resulting reaction forces are obtained, which are used to update the attitude angle iteratively until convergence is achieved (as per Equation 12). The final converged pressure distribution is then used to compute the LCC. Hence, although eccentricity ratio is used as an input, the computed LCC serves as a performance output, allowing comparative evaluation of different groove configurations under identical journal positions.

$$\bar{Z}_0 = \left| \frac{\left[p_t{}^{-m'}\right] - \left[p_t{}^{-(m'-1)}\right]}{\left[p_t{}^{-(m'-1)}\right]} \right| \times 100 \leq TLM \tag{12}$$

Before moving ahead, a mesh size testing is carried out to finalize the grid size. The calculation of load carrying capacity (LCC) for a rectangular macro-groove bearing with four grooves, groove depth $\bar{d}_g$ of 0.6 and eccentricity ratio 0.6 has been chosen under several mesh densities, as illustrated in Figure 5(a). However, above a certain level of improvement in LC the processing time increases significantly without a significant improvement in the accuracy of the result as shown in Figure 5(b). Therefore, in the present study, the macro-grooved hydrodynamic journal-bearing (MGHJB) system can reach the desired level of precision with 1,170 mesh density elements i.e 65 × 18 elements in circumferential and axial direction is used in the current study.

4.0 RESULTS AND DISCUSSION

The static characteristics are determined for the bearing with rectangular macro-groove textures considering the effect of groove depth, number, area density and the regions at the eccentricity ratios of 0.2 to 0.8. The MATLAB code developed for the present study is validated with the published data by (Chandrawat and Sinhasan, 1987; Awasthi et al., 2006; Sharma et al., 2021) as shown in Table 1. Further a comparative analysis was performed between the present numerical study and the experimental results reported by Filgueira Filho et al., 2021 to validate the performance of the plain journal bearing model. The calculated Sommerfeld number and attitude angle values exhibit strong agreement with the experimental data, as illustrated in Figures 6(a) and 6(b). Further, the static and dynamic parameters of bearing with rectangular shaped macro-grooves of the present study are compared with existing numerical simulations studies with different micro and macro-textured profile shapes. Table 2 shows the present results compared with four number of textures with a depth of 0.6 placed in the pressure increasing region with chevron shape textures (Sharma et al., 2019; Jamwal et al., 2020) and rectangular, and arc shaped textures (Byotra and Sharma, 2023). The simulation results of the present study are found to be consistent with published results, thereby validating the MATLAB programme used in the current study and the difference in results may be due to different shapes of textures, different adopted numerical techniques and mesh sizes. This consistency confirms the accuracy of the current numerical approach and establishes it as a reliable basis for further investigations in this study.

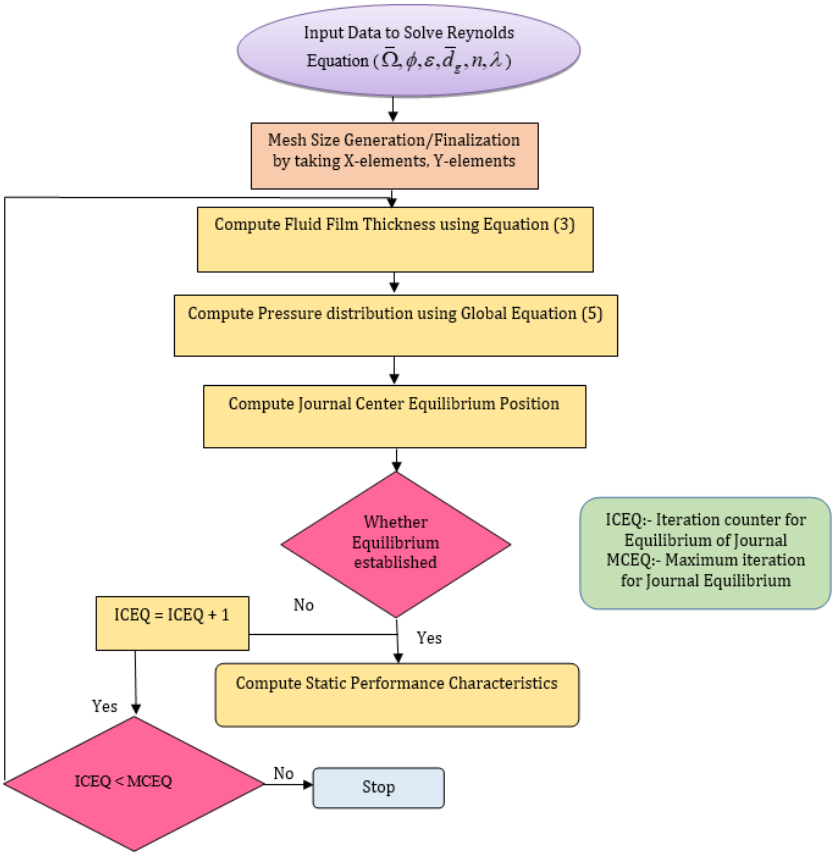

Figure 4: Illustration of the overall solution process.

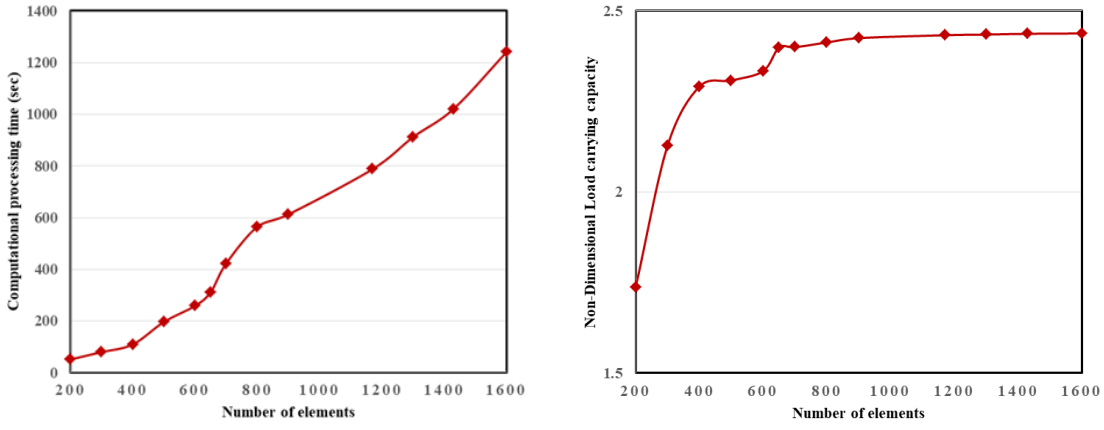

(a) (b)

Figure 5: (a) Load-carrying capacity (LCC) (b) Processing time versus no. of elements to get optimal mesh size.

For the current study the operating and geometric parameters are shown in Table 3. The following bearing regions as defined by equation 4 have been chosen to place the rectangular shaped macro-groove textures as depicted in Figure 3(a)–(d):-

a) Full Circumferential region (0°-360°)
b) First half region (0°-180°)
c) Second half region (180°-360°)
d) Pressure-increasing region (144°-288°)

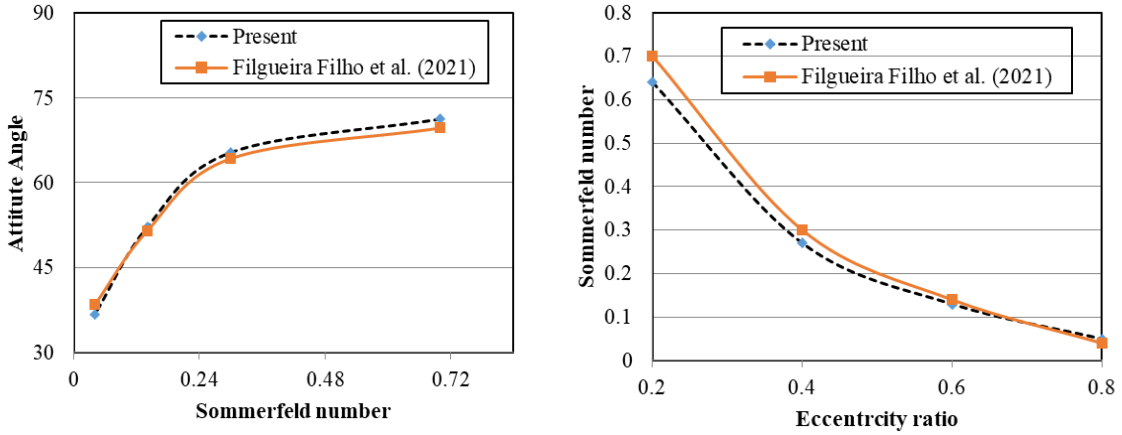

(a) (b)

Figure 6: Comparison between present results and experimental data from Filgueira Filho et al., 2021: (a) Sommerfeld number vs. eccentricity ratio, (b) Sommerfeld number vs. attitude angle.

Each rectangular groove is located in the bearing surface with a flat bottom surface. The maximum four grooves are considered on the bearing surface in current study. In case of full surface of the bearing (0–360°), the first groove will occupy location initially from 0° to 90°, and then second will occupy 90° to 180°, after that third groove will lie in 180° to 270° and finally fourth groove will lie in 270° to 360°. Hence, the total length of the unit cell (L_α) in circumferential direction for one groove is (0–90°) or 1.571 radians. The total dimensions in axial directions of the groove is considered as L_β (-1 to +1). The dimension 'a' and 'b' has been set as margins in the circumferential and axial directions respectively and its values are taken initially as 12.5% of L_α and 12.5% of L_β. Hence the groove length in the circumferential direction (G_α) is initially taken as 75% of the cell dimension (L_α) and Groove width (G_β) is taken as 75% of the cell dimension (L_β) in the axial direction in different regions as shown in Figure 3(a)–(d). The ratio of the area covered by the macro-groove to the entire area where the groove/macro-texture is applied may be used to compute the texture area density (A_d), which is calculated by using the following equation:-

$$A_d = \frac{\text{Area acquired by groove}}{\text{Total area considered for groove}} \times 100 \qquad (13)$$

4.1 Full Macro-groove Distribution in Circumferential Direction (0°-360°)

For rectangular macro-grooves distribution in the full region of bearing, it was found that the load-carrying capacity (LCC) is reduced at various groove number, depth, and eccentricity ratios while friction coefficient (FC) is enhanced in comparison with plain journal bearing. Table 4 and 5 depict that providing macro-grooves in full region has a negative effect on the static characteristics of the bearing. The most optimistic outcome was found at n=1, $\bar{d}_g$ = 1.5, and eccentricity ratio of 0.2, where LCC enhances by 5.25% and FC reduces by 1.35%, while most negative impact were found at n=1, $\bar{d}_g$= 1.5, and ε = 0.8, where LCC reduces by 5.34% and FC increases by 1.39%. It was further observed that the most negative impact of macro-grooved bearing was found at a higher eccentricity ratio. The reason for decrease in LCC and increase in FC may be due to presence of macro-grooves on the bearing surface, the flow rate increases due to the formation of a lubricant reservoir which further reduces the pressure and increases film thickness in the clearance space. The grooves in the diverging region allow more lubricants to accumulate, increasing the film thickness but reducing the pressure build up due to lower hydrodynamic wedge action—resulting in decreased LCC and increased viscous friction.

4.2 First Half Macro-groove (0°-180°)

For rectangular macro-grooves distribution in the first half region of bearing, it was found from Table 4 and 5 that this configuration has also a detrimental effect on the LCC and FC for different values of grooves, groove depth, operating under different values of eccentricity ratio. The most optimistic results for this type of configuration were found at n=1, $\bar{d}_g$ = 0.3, and eccentricity ratio of 0.2, where LCC reduces by 5.63% and FC increase by 5.87% , while most negative impact were found at n=2, $\bar{d}_g$= 1.5, and eccentricity ratio of 0.2, where LCC reduces by 81.63% and FC increases by 49.49%. It was further observed that the most discrete reduction of results was found at a lower eccentricity ratio at higher groove depth while the least negative results were again at a lower eccentricity ratio but lower groove depth.

4.3 Second Region Macro-groove (180°-360°)

For this type of groove distribution in the second half region of bearing, Table 4 and 5 depict that this configuration also reduces the bearing's characteristics as LCC decreases and FC increases in comparison with smooth plain bearing. Furthermore, it was noted that for all eccentricity ratio values, the macro-groove in 0-180° region yield good results than 180-360° region since the LCC in first half is higher than the value of LCC in second half for different groove number and depth. The most optimistic results for this type of configuration were found at n=2, $\bar{d}_g$= 0.9, and ε=0.2, where LCC reduces by 12.93% and FC increases by 14.06%, while discrete reduction of results were found at n=2, $\bar{d}_g$= 1.5, ε=0.8, where LCC reduces by 72.37% and FC increases by 225.41%. It was further observed that at high eccentricity ratio and groove depth the results were negative while at low eccentricity ratio and high groove depth the results were least negative. The reason for decrease in LCC and increase in FC in this region is that due to macro-grooves in the diverging zone on the bearing surface, more lubricant flow inside the clearance space which makes a lubricant reservoir. Hence lubricant film thickness will increase between journal and the bearing which leads to the development of low pressure.

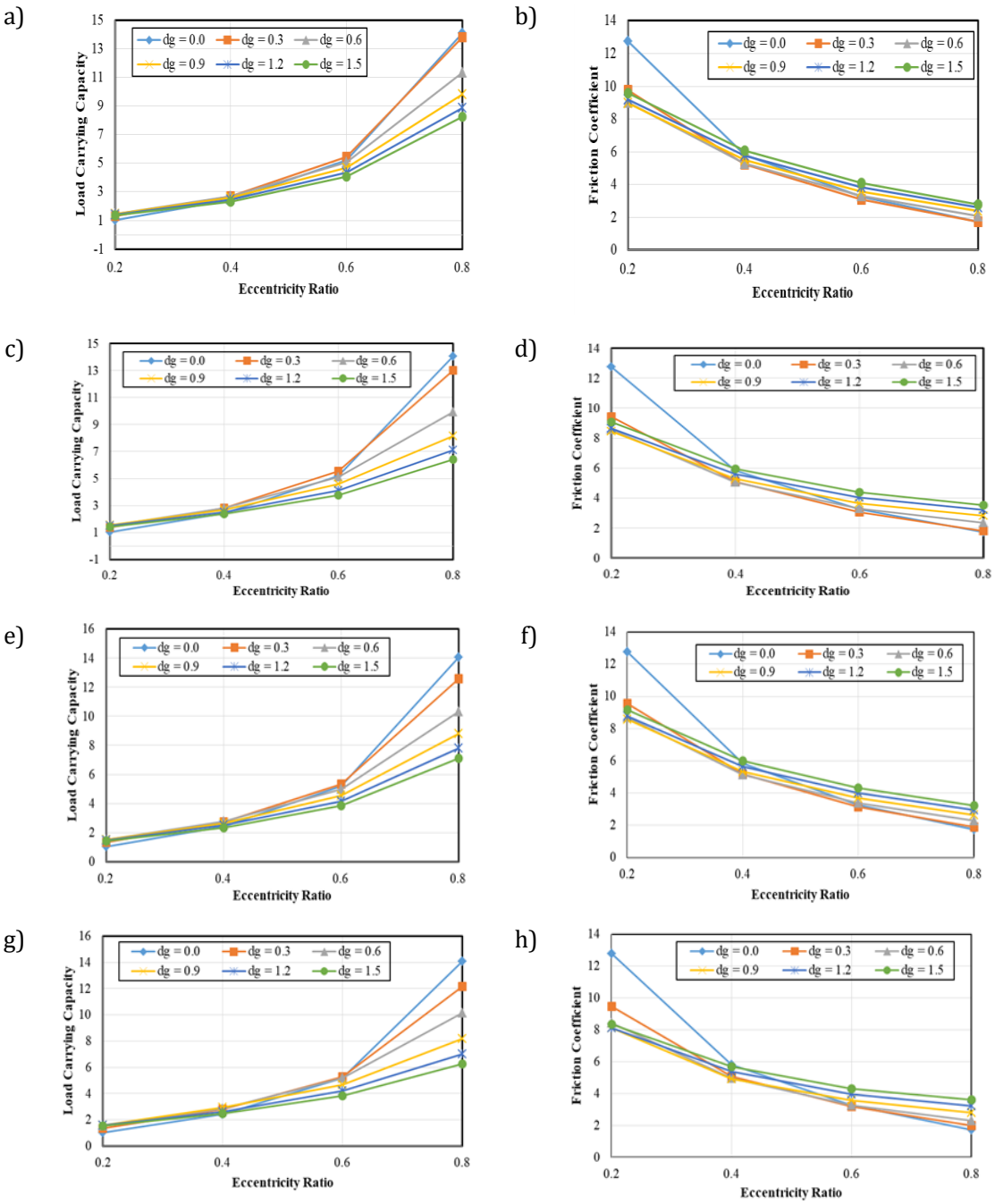

Figure 7: Variation of load capacity (LC) and friction coefficient (FC) with rectangular macro-grooves in pressure enhancing region at different eccentricity ratios and macro-groove depth with (a)- (b) one macro-groove (c)- (d) two macro-grooves (e)- (f) three macro-grooves (g)- (h) four macro-grooves.

4.4 Rectangular Macro-groove in the Pressure-enhancing Region (144°-288°)

For rectangular macro-grooves placed on the bearing inner surface zone between 144°-288° region, Tables 4 and 5 and Figure 7 (a-h) shows the variation in LCC and FC at different eccentricity ratio with one to four number of macro-groove and non-dimensional groove depths $\bar{d}_g$= 0.3-1.5. The results depict that this type of configuration enhances the performance of bearing as LCC increases and FC decreases at low and high eccentricity ratios, at different groove number and depth in comparison with plain bearing. It was observed that at ε=0.2, LCC enhances and FC decreases with an increase in the groove number and groove depth upto $\bar{d}_g$= 0.9 in this region. As depicted in Figure 7 (a-b), with one macro-groove in pressure enhancing region i.e at n=1 the greatest improvement of LCC is 42.64%, while FC reduces by 29.68% at ε=0.2 and, $\bar{d}_g$= 0.9. At n=2, the maximum LCC is 51.62% and minimum FC is 33.85% at ε=0.2 and, $\bar{d}_g$= 0.9 as depicted in Figure 7 (c-d), while at n=3, the maximum LCC is 49.35% and minimum FC is 3.86% as shown in Figure 7 (e-f) at ε=0.2 and, $\bar{d}_g$= 0.9. For four macro-grooves at n=4, ε=0.2 and, $\bar{d}_g$= 0.9, LCC increases by 57.95% and FC reduces by 36.51% as shown in Figure 7 (g)–(h) in comparison with plain bearing. At ε=0.4, the value of LCC increases and FC decreases with increasing the number of groove and depth and the maximum enhancement in LCC is 20.29% and reduction in FC is 15.75% at n=4, $\bar{d}_g$= 0.9. At ε=0.6, it was found that LCC and FC decreases with enhancement in groove number in this region, the maximum value of LCC and FC was found at low groove depth. The maximum enhancement in LCC is 6.15% and the reduction in FC is 5.77% at n=2, $\bar{d}_g$= 0.3.

The reason being that when macro- are introduced in the pressure-building zone (typically the converging region) and designed with optimal dimensions (area and depth), they act as pressure boosters. The presence of these cavities modifies the local geometry of the clearance space, allowing the journal to momentarily deflect toward the groove. This leads to a localized reduction in film thickness, increasing pressure due to enhanced wedge formation. Consequently, this results in higher LCC and reduced COF. But at higher eccentricity ratio, ε=0.8, the presence of macro groove has negative effects on the performance of bearing. It is established that the performance of the bearing is maximum at higher number of macro-groove at large value of the grove depth at low eccentricity ratio while by enhancing the eccentricity ratio the performance of bearing is found better only at lower number of macro-grooves with low groove depth. The results further show that positive effect of macro-groove on bearing performance is found at lower eccentricity ratios. The outcomes completely concur with the published findings (Sharma et al., 2021; Jamwal et al., 2020).

4.5 Optimum Parameters of Rectangular Macro-groove Texturing in the Pressure-enhancing Region (144°-288°)

Further, an effort is being made to improve bearing performance by altering the area density of the rectangular macro-groove by varying the values of G_α and G_β in pressure enhancing region. It was found that in case of four rectangular macro-grooves in pressure enhancing region with initial groove length in the circumferential direction (G_α) taken as 75% of the cell dimension (L_α) and groove width (G_β) as 75% of the cell dimension (L_β) in the axial direction with area density of 56.25% and $\bar{d}_g$= 0.9, and at ε=0.4, the maximum enhancement in LCC is 20.29% and reduction in FC is 15.75%. The optimum value of the groove length in the circumferential direction (G_α) was found as 90% of the cell dimension (L_α) and Groove width (G_β) as 65% of the cell dimension (L_β) in the axial direction and with area density of 58.50 %, there is enhancement of LCC as 27.78% and reduction in FC as 21.36% with $\bar{d}_g$= 0.9, at ε=0.4. The outcomes corresponding to the optimal

parameters of macro-groove agree with the published results of Kango et al. (2014). The optimal dimensions of the four rectangular macro-grooves placed on the inner surface of bearing in terms of length, width and depth (in millimeter) at different eccentricity ratios (0.2 and 0.4) are 31.05 mm, 65 mm and 0.045 mm respectively. The groove depth of 0.045 mm (or 45 microns) is substantially larger than micro-textures, which are generally in the range of 1–10 microns. Thus, the adopted geometry of macro-groove clearly falls under macro-texturing. Hence, the optimal total length of the rectangular shaped macro-groove is 35.94% of the circumferential length of the bearing, while the total width of the groove is 65% of the axial length of the bearing. Table 6 shows the optimal dimensions of rectangular macro-groove in millimeter (mm). This parametric optimization was performed to avoid excessive groove dimensions, which could otherwise impair pressure development and reduce the load-carrying capacity (LCC), while too shallow or short grooves may offer negligible hydrodynamic advantage.

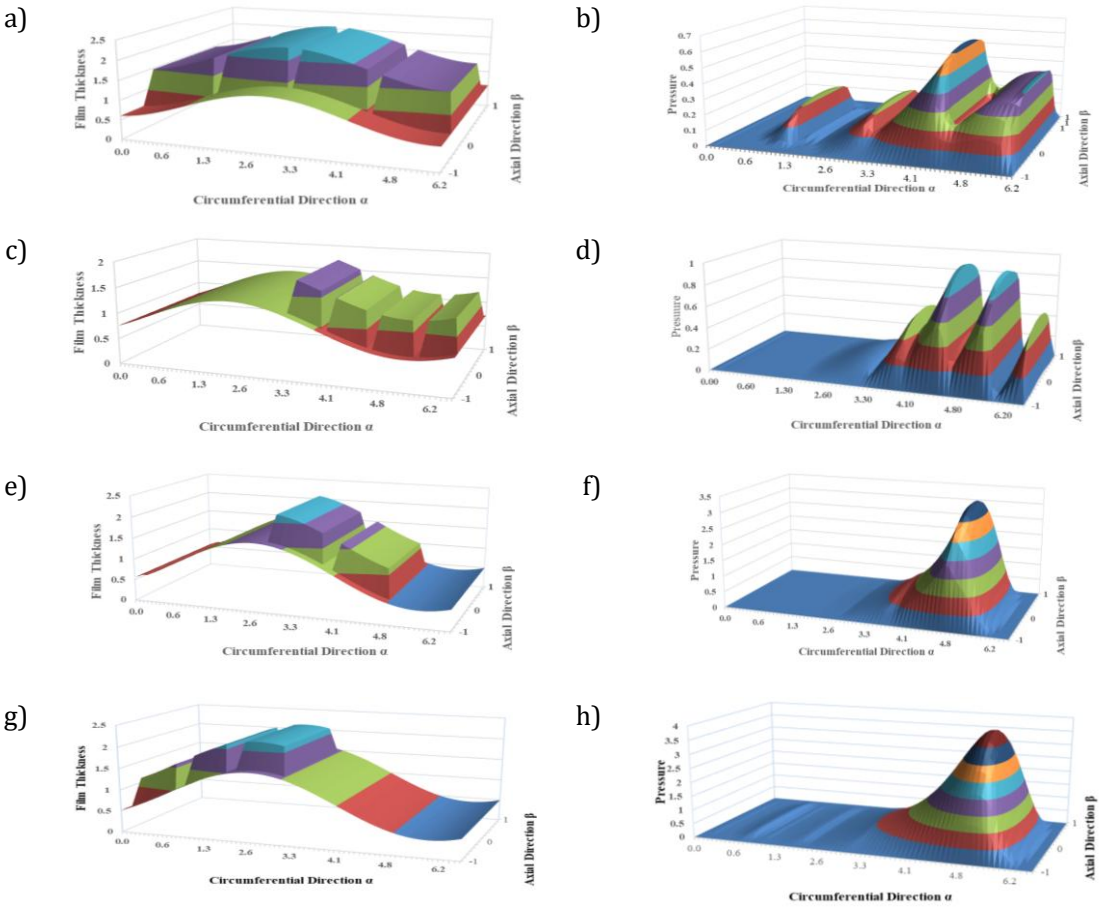

Figure 8: Non-dimensional film thickness and pressure curve for bearing with (a) Four macro grooves in full region at groove depth of 0.9; (b) Four macro grooves in second half region at groove depth of 0.6; (c) Two macro grooves in pressure increasing region at groove depth of 0.6; (d) Three macro grooves in first half region at groove depth of 0.6 and eccentricity ratio of 0.4.

With these optimum parameters and area density of 58.50 %, the performance of bearing is further enhanced with maximum enhancement of LCC is 95.75% and reduction in FC is 48.67% at n=4, $\bar{d}_g$= 0.9 at eccentricity ratio, ε=0.2. While at eccentricity ratio of 0.4, n=4, $\bar{d}_g$= 0.9, LCC enhances by 27.78% and FC reduces by 21.36% and at ε=0.6, n=2, $\bar{d}_g$= 0.3, LCC enhances by 7.94% and FC reduces by 8.54%. However, at higher eccentricity ratio of 0.8, the promotion of macro-groove texture, the maximum performance was found at optimum geometry of one groove in pressure increasing region, at depth of 0.3, as LCC enhances by 1.72% and reduction in FC is 1.46%.

The pressure profiles illustrate how the pressure distribution varies across the bearing surface. These variations are influenced by the number, groove depth, area density and region. Similarly, the thickness profiles represent the film thickness across the bearing surface, crucial for maintaining lubrication and preventing metal to metal contact. The Figures 8 (a) – (d) presents a three-dimensional representation of pressure distribution as a function of the circumferential direction (α) and axial direction (β) due to the presence of rectangular macro-grooves in the various regions of the bearing surface.

5.0 CONCLUSION

In the present study, authors have investigated the static characteristics of the journal bearing considering the impact of rectangular macro-groove textures in the different regions by varying the groove number, depth and area density. The computed findings discussed in the sections make the following evident conclusions:

(1) Among all the regions taken into consideration for the analysis of MGHJB by providing rectangular macro-grooves, the pressure-enhancing region yielded the maximum static characteristics of the bearing.
(2) At low eccentricity ratio 0.2, with four grooves, and groove depth 0.9, with area density of 58.51%, the bearing's load capacity (LC) increased by 95.75% and its friction coefficient (FC) decreased by 48.67%.
(3) However, at higher eccentricity ratio of 0.8, the promotion of macro-groove texture, the maximum performance was found at optimum geometry of one groove in pressure increasing region, at depth of 0.3, as LCC enhances by 1.72% and reduction in FC is 1.46.
(4) It is established that the performance of the bearing is maximum at low eccentricity ratio with higher number of macro-groove at large value of the grove depth while by enhancing the eccentricity ratio the performance of bearing is found better only at lower number of macro-grooves with low groove depth.
(5) However, to fully understand the mechanisms driving these improvements, further experimental investigations are necessary. This will provide more detailed insights into the optimization of macro-grooves geometry for journal bearing systems in advanced engineering applications.

ACKNOWLEDGEMENT

The authors gratefully acknowledge the support of School of Mechanical Engineering, Shri Mata Vaishno Devi University, Jammu and Kashmir, INDIA.

NOMENCLATURE

Dimensional parameters

c_r= Radialclearance,mm;
D_j = Diameter of Journaldiamter,mm;
d_g= Macro-groove depth,mm;
e_j = Eccentricity of Journal,mm;
W_b = Load carrying capacity of bearing ($\partial h/\partial t \neq 0$),N;
W_X, W_Z = Load carrying capacity components($\partial h/\partial t \neq 0$),N;
F_L = Frictional Force,N;
f = Friction Coefficient;
t = time, sec;
h= fluid film thickness,mm;
h_g= variation in h due to macro-groove,mm;
L_b= Length of Bearing,mm;
N_s= Speed (Rotational) of Journal,rpm;
p_t= Pressure, N/mm^2;
p_{st}= Pressure of lubricant supply, N/mm^2($\mu_r \omega_j {R_j}^2/{c_r}^2$);
Q_t= Flow of lubricant,mm^3.sec^{-1}
R_j, R_b= Journal and bearing radius,mm;
W= Applied load on bearing,N;
x, y, z= Circumferential, Axial coordinates,andalong film thickness,mm;
$X_j Z_j$= Center coordinate of Journal;

Non-dimensional parameters

$\bar{c}$ $= c_r/R_j$;
$\bar{F}_0, \bar{F}_1, \bar{F}_2$ = Viscosity functions;
$\bar{h}$ $= h/c_r$;
$\bar{h}_{\min}$ $= h_{\min}/c_r$;
$\bar{p}_t, \bar{p}_{\max}$ $= p_t/p_{st},\ p_{\max}/p_{st}$;
$\bar{t}$ $= tc_r^2 p_{st}/\mu_r R_j^2$;
$\bar{W}, \bar{W}_0$ $= W/p_{st}R_j^2, W_0/p_{st}R_j^2$;
$\bar{W}_x, \bar{W}_z$ $= W_x/p_{st}R_j^2, W_z/p_{st}R_j^2$;
$\bar{X}_j, \bar{Z}_j$ $= X_j/c_r,\ Z_j/c_r$;
$\bar{x}, \bar{z}$ $= x/c_r,\ z/c_r$;
α, β $= x/R_j, y/R_j$;
$\bar{d}_g$ $= d_g/c_r$;
ε $=$ Eccentricity ratio (e_j/c_r);
n $=$ number of macro-groove;
$\bar{\Omega}$ $= \omega\mu_r R_j^2/c_r^2 p_{st}$

Greek letters

μ_0 = Viscosityof baselubricant Ns/m^2;
ω_j = Journalrotational speed rad/sec,mm;
ϕ= Attitude angle,rad;
λ= Aspect ratio, (L_b/D$_b$)

Vectors and matrices

$[\bar{F}_M]$= Liquidity matrix;
$[\bar{N}_M]$= Matrix for Shape function;
$\{\bar{p}_V\}$= Vector for Nodal pressure;
$\{\bar{Q}_V\}$= Vector for Nodal flow;
$\{\bar{R}_X, \bar{R}_Z\}$= Vectors RHS due to center velocity of journal;
$\{\bar{R}_H\}$= Hydrodynamic Column vector;

REFERENCES

Adatepe, H., Bıyıklıoglu, A., & Sofuoglu, H. (2013). An investigation of tribological behaviors of dynamically loaded non-grooved and micro-grooved journal bearings. Tribology International, 58, 12-19.

Arif, M., Kango, S., & Shukla, D. K. (2022). Analysis of textured journal bearing with slip boundary condition and pseudoplastic lubricants. International Journal of Mechanical Sciences, 228, 107458.

Ashihara, K., & Hashimoto, H. (2010). Theoretical modeling for microgrooved journal bearings under mixed lubrication.

Awasthi, R. K., Jain, S. C., & Sharma, S. C. (2006). Finite element analysis of orifice-compensated multiple hole-entry worn hybrid journal bearing. Finite Elements in Analysis and Design, 42(14-15), 1291-1303.

Bangotra, A., & Sharma, S. (2022). Impact of surface waviness on the static performance of journal bearing with CuO and CeO2 nanoparticles in the lubricant. Industrial Lubrication and Tribology, 74(7), 853-867.

Bangotra, A., & Sharma, S. (2023). Impact of partial surface waviness on the tribological performance of hydrodynamic journal bearing. Lubrication Science, 35(3), 207-224.

Byotra, D., & Sharma, S. (2023). Effect of texture shapes and additives in lubricants on the dynamic characteristics of the hydrodynamic journal bearing. Industrial Lubrication and Tribology, 75(9), 1031-1044.

Chandrawat, H. N., & Sinhasan, R. (1987). A comparison between two numerical techniques for hydrodynamic journal bearing problems. Wear, 119(1), 77-87.

Chen, Y., Feng, J., Sun, Y., Peng, X., Dai, Q., & Yu, C. (2020). Effect of groove shape on the hydrodynamic lubrication of journal bearing considering cavitation. Engineering Computations, 37(5), 1557-1576.

Feng, H., Jiang, S., & Shang-Guan, Y. (2021). Three-dimensional computational fluid dynamic analysis of high-speed water-lubricated hydrodynamic journal bearing with groove texture considering turbulence. Proceedings of the Institution of Mechanical Engineers, Part J: Journal of Engineering Tribology, 235(11), 2272-2286.

Filgueira Filho, I. C. M., Bottene, A. C., Silva, E. J. D., & Nicoletti, R. (2021). Static behavior of plain journal bearings with textured journal-experimental analysis. Tribology International, 159, 106970.

Fu, Y., Ji, J., & Bi, Q. (2012). The influence of partially textured slider with oriented parabolic grooves on the behavior of hydrodynamic lubrication. Tribology Transactions, 55(2), 210-217.

Gui, C., & Meng, F. (2019). Comparative study of spherical dimple and bump effects on the tribological performances of journal bearing. Proceedings of the Institution of Mechanical Engineers, Part J: Journal of Engineering Tribology, 233(1), 139-157.

Jamwal, G., Sharma, S., & Awasthi, R. K. (2020). The dynamic performance analysis of chevron shape textured hydrodynamic bearings. Industrial Lubrication and Tribology, 72(1), 1-8.

Kango, S., Sharma, R. K., & Pandey, R. K. (2014). Comparative analysis of textured and grooved hydrodynamic journal bearing. Proceedings of the Institution of Mechanical Engineers, Part J: Journal of Engineering Tribology, 228(1), 82-95.

Khatri, C. B., & Sharma, S. C. (2016). Influence of textured surface on the performance of non-recessed hybrid journal bearing operating with non-Newtonian lubricant. Tribology International, 95, 221-235.

Kumar, V., & Sharma, S. C. (2019). Effect of geometric shape of micro-grooves on the performance of textured hybrid thrust pad bearing. Journal of the Brazilian Society of Mechanical Sciences and Engineering, 41, 1-24.

Li, P., Zeng, F., Xiao, S., Zhen, D., Zhang, H., & Shi, Z. (2021). Effects of texture bottom profile on static and dynamic characteristics of journal bearings. Shock and Vibration, 2021(1), 7068744.

Manser, B., Belaidi, I., Hamrani, A., Khelladi, S., & Bakir, F. (2019). Performance of hydrodynamic journal bearing under the combined influence of textured surface and journal misalignment: A numerical survey. Comptes Rendus Mécanique, 347(2), 141-165.

Pattnayak, M. R., Pandey, R. K., & Dutt, J. K. (2022). Performance improvement of an oil-lubricated journal bearing using bionic-textures fused micro-pockets. Journal of Tribology, 144(4), 041804.

Qiu, M., Minson, B. R., & Raeymaekers, B. (2013). The effect of texture shape on the friction coefficient and stiffness of gas-lubricated parallel slider bearings. Tribology International, 67, 278-288.

Rahmani, F., Pandey, R. K., & Dutt, J. K. (2018). Performance studies of powder-lubricated journal bearing having different pocket shapes at cylindrical bore surface. Journal of Tribology, 140(3), 031704.

Rao, T. V. V. L. N., Abdul-Rani, A. M., Thirumalaiswamy, N., & Hashim, F. M. (2013). Load capacity of partially textured journal bearing with trapezoidal recess. Applied Mechanics and Materials, 315, 830-834.

Sahu, K., & Sharma, S. C. (2018). A study on performance of slot entry hybrid journal bearing considering effect of surface irregularities. Industrial Lubrication and Tribology, 70(6), 1094-1109.

Sharma, S. C., Phalle, V. M., & Jain, S. C. (2012). Performance of a noncircular 2-lobe multirecess hydrostatic journal bearing with wear. Industrial Lubrication and Tribology, 64(3), 171-181.

Sharma, S. C., & Kushare, P. B. (2017). Nonlinear transient response of rough symmetric two lobe hole entry hybrid journal bearing system. Journal of Vibration and Control, 23(2), 190-219.

Sharma, S., Jamwal, G., & Awasthi, R. K. (2019). Enhancement of steady state performance of hydrodynamic journal bearing using chevron-shaped surface texture. Proceedings of the

Institution of Mechanical Engineers, Part J: Journal of Engineering Tribology, 233(12), 1833-1843.
Sharma, S., Jamwal, G., & Awasthi, R. K. (2020). Dynamic and stability performance improvement of the hydrodynamic bearing by using triangular-shaped textures. Proceedings of the Institution of Mechanical Engineers, Part J: Journal of Engineering Tribology, 234(9), 1436-1451.
Sharma, S., Sharma, A., Jamwal, G., & Kumar Awasthi, R. (2021). The effect of V-shape protruded and dimple textured on the load-carrying capacity and coefficient of friction of hydrodynamic journal bearing: A comparative numerical study. Proceedings of the Institution of Mechanical Engineers, Part J: Journal of Engineering Tribology, 235(5), 997-1011.
Sharma, S. C., & Tomar, A. K. (2021). Study on MR fluid hybrid hole-entry spherical journal bearing with micro-grooves. International Journal of Mechanical Sciences, 202, 106504.
Shinde, A. B., & Pawar, P. M. (2017). Effect of partial grooving on the performance of hydrodynamic journal bearing. Industrial Lubrication and Tribology, 69(4), 574-584.
Singh, N., & Awasthi, R. K. (2022). Influence of surface textures on the dynamic stability and performance parameters of hydrodynamic two-lobe journal bearings. Proceedings of the Institution of Mechanical Engineers, Part J: Journal of Engineering Tribology, 236(8), 1589-1602.
Tala-Ighil, N., Fillon, M., & Maspeyrot, P. (2011). Effect of textured area on the performances of a hydrodynamic journal bearing. Tribology International, 44(3), 211-219.
Uddin, M. S., & Liu, Y. W. (2016). Design and optimization of a new geometric texture shape for the enhancement of hydrodynamic lubrication performance of parallel slider surfaces. Biosurface and Biotribology, 2(2), 59-69.
Wang, C. C., & He, C. L. (2019). Numerical study of a hydrodynamic journal bearing with herringbone grooves for oil leakage reduction. Proceedings of the Institution of Mechanical Engineers, Part J: Journal of Engineering Tribology, 233(3), 439-446.
Yu, R., Chen, W., & Li, P. (2016). The analysis of elastohydrodynamic lubrication in the textured journal bearing. Proceedings of the Institution of Mechanical Engineers, Part J: Journal of Engineering Tribology, 230(10), 1197-1208.
Zhang, P., Qian, Y., & Qian, Q. (2021). Multi-objective optimization for materials design with improved NSGA-II. Materials Today Communications, 4(2), 1-7.
Zhang, X., Liu, C., & Zhao, B. (2021). An optimization research on groove textures of a journal bearing using particle swarm optimization algorithm. Mechanics & Industry, 22, 1.